Crystal-Chemical Characteristics of Silicon−Neodymium Substituted Hydroxyapatites Studied by Combined X-ray and Neutron Powder Diffraction

D. Arcos,*[,†,‡] J. Rodríguez-Carvajal,[‡] and M. Vallet-Regí[†]

Departamento Química Inorgánica y Bioinorgánica, Facultad de Farmacia, Universidad Complutense, 28040-Madrid, Spain, and Laboratoire Léon Brillouin (CEA-CNRS), CEA/Saclay, 91191 Gif sur Yvette Cedex, France

Received July 20, 2004. Revised Manuscript Received October 13, 2004

Neodymium−silicon britholites, $Ca_{10-x}Nd_x(PO_4)_{6-x}(SiO_4)_x(OH)_2$, have been synthesized by the ceramic method. These materials can be used as host matrixes for actinides immobilization and Nd models the actinide. The crystal-chemistry evolution as a function of the Si and Nd content has been studied by combined neutron and X-ray Rietveld refinement. The SiO_4^{4-} substitution for PO_4^{3-} does not lead to significant changes in the PO_4 tetrahedrons. The Nd^{3+} cations substitute for Ca^{2+} and are placed at the Ca(2) sites, getting closer to the hydroxyl sites. The local increase of positive charge around hydroxyls leads to the O^{2-} stabilization in 4e Wyckoff position. Since neutrons are sensitive to the H atoms, the hydroxylation degree has been calculated. Finally, the scattering density Fourier difference maps suggest the presence of HPO_4^{2-} groups, which partially substitute for PO_4^{3-} to keep the electric balance of these compounds.

Introduction

Britholites are phospho-silicate apatites having the general composition $Ca_{10-y}(RE)_y(SiO_4)_y(PO_4)_{6-y}(F,OH)_2$ where RE are rare earth elements.[1,2] These materials have interest for the management of long-lived and high-activity radioactive wastes. Studies of natural apatites from the fossil nuclear reactor of Oklo showed that these compounds support high doses of external and internal α irradiation, without undergoing important changes in the crystal structure.[3,4]

Neodymium−silicon substituted hydroxyapatite, a britholite $Ca_{10-x}Nd_x(PO_4)_{6-x}(SiO_4)_x(OH)_2$, is considered as a potential host matrix for the specific immobilization of actinides. In this case, Nd is used to model the trivalent actinides due to their similar chemical properties.[5] Studies carried out over $Ca_9Nd(PO_4)_5SiO_4F_2$ have shown that this compound allows the incorporation of 10 wt. % of actinides, they are not affected by disruption of the crystal lattice, and they can anneal the defects created by self-irradiation.[6]

The structure of hydroxylapatite (HA) can be described as a hexagonal unit cell with space group $P6_3/m$ and lattice parameters $a = 9.432$ Å and $c = 6.881$ Å, having one formula unit $Ca_{10}(PO_4)_6(OH)_2$ per unit cell.[7] The hydroxyls ions and four Ca ions at Ca(1) sites lie along columns parallel to the *c* axis. The hydroxyls are sited along the *c* axis and the O−H bond direction is parallel to it, without straddling the mirror planes at $z = {}^1/_4$ and ${}^3/_4$. The remaining six Ca atoms, positioned at Ca(2) sites, are associated with the two hydroxyl groups in the unit cell, where they form triangles centered on, and perpendicular to, the OH axis and laying on the mirror planes. The PO_4 tetrahedrons form the remaining basic structural unit of HA. This structure allows several substitutions[8−12] and neodymium−silicon britholites can be understood as HA where Nd^{3+} substitutes for Ca^{2+} and SiO_4^{4-} substitutes for PO_4^{3-}. In this sense, structural studies of neodymium and lanthanum britholites have been reported by Boyer et al.[13,14]

When using diffraction techniques to study the crystal-chemistry of silicon and neodymium britholites, several items must be taken into account. For example, the scattering factors of P and Si for X-rays are almost identical. Moreover, light atoms such as H cannot be detected with this radiation. Although XRD provides valuable structural information, a

* To whom correspondence should be addressed. E-mail: arcos@llb.saclay.cea.fr.
† Universidad Complutense.
‡ Laboratoire Léon Brillouin (CEA-CNRS).

(1) Meis, C.; Gale, J. D.; Boyer, L.; Carpena, J.; Gosset D. *J. Phys. Chem.* **2000**, *104*, 5380.
(2) Boyer, L.; Piriou, B.; Carpena, J.; Lacout, J. L. *J. Alloys Compd.* **2000**, *311*, 143.
(3) Bros, R.; Carpena, J.; Sere V.; Beltritti, A. *Radiochim. Acta* **1996**, *74*, 277.
(4) Carpena, J.; Sere, V. In *Proceedings of the Fourth Joint EC−CEA Final Meeting*, Saclay, France, Nuclear Science Technology Series; European Commision, 1995; Blanc, P. L., von Maravic, M., Eds.; pp 225−238.
(5) Brégiroux, D.; Audubert, F.; Champion, E.; Bernache-Assollant, D. *Mater. Lett.* **2003**, *57*, 3526.
(6) Utsunomiya, S.; Yudintsev, S.; Wang, L. M.; Ewing, R. C. *J. Nucl. Mater.* **2003**, *322*, 180.
(7) Kay, M. I.; Young, R. A.; Posner, A. S. *Nature* **1964**, *204*, 1050.
(8) Arcos, D.; Rodríguez-Carvajal, J.; Vallet-Regí, M. *Chem. Mater.* **2004**, *16*, 2300.
(9) Ergun, C.; Webster, T. J.; Bizios, R.; Doremus, R. H. *J. Biomed. Mater. Res.* **2002**, *59*, 305.
(10) Webster, T. J.; Ergun, C.; Doremus, R. H.; Bizios, R. *J. Biomed. Mater. Res.* **2002**, *5*, 312.
(11) Elliott, J. C.; Bonel, G.; Trombe, J. C. *J. Appl. Crystallogr.* **1980**, *13*, 618.
(12) Wilson, R. M.; Elliott, J. C.; Dowker, S. E. P. *Am. Mineral.* **1999**, *84*, 1406.
(13) Boyer, L.; Savariault, J. M.; Carpena, J.; Lacout, J. L. *Acta Crystallogr.* **1998**, *C54*, 1057.
(14) Boyer, L.; Carpena, J.; Lacout, J. L. *Solid State Ionics* **1997**, *95*, 121.

10.1021/cm0488231 CCC: $30.25
Published on Web 12/07/2004

full understanding of the britholites structure requires additional techniques. On the other hand, neutron diffraction techniques have been demonstrated to be useful to study the silicon incorporation into hydroxyapatite.[15−17] Moreover, neutrons are very sensitive to H atoms, but hardly distinguish Nd from Ca.

In this work, we deal with the structural and chemical variation of Nd−Si substituted hydroxyapatites obtained by high-temperature synthesis. It is difficult to determine the composition at the *4e* Wyckoff position because the hydroxyls groups partially decompose over 850 °C, resulting in oxy-hydroxylapatites.[18−20] It is well-known that the local composition at the *4e* site is very important for the stability of the apatites.[7,21] In this work, we combine neutron and X-ray powder diffraction to study these materials. The understanding of the crystal-chemistry of britholites can help us to tailor better host matrixes for nuclear waste storage.

Experimental Section

Silicon−neodymium-substituted hydroxylapatites (britholites) of general formula $Ca_{10-x}Nd_x(PO_4)_{6-x}(SiO_4)_x(OH)_2$, have been synthesized by the traditional ceramic method. Britholites with $x = 0$, 0.5, and 1 (samples B-0, B-0.5, and B-1, respectively) were obtained by mixing stoichiometric amounts of $CaCO_3$, Nd_2O_3, $Ca_2P_2O_7$, and SiO_2. The powder mixtures were pre-fired at 900 °C for 1 h, ground, and shaped into disks by uniaxial pressure. Finally, the disks were treated at 1200 °C for 24 h under air atmosphere. The samples were quenched from high to room temperature.

Fourier transform infrared (FTIR) spectra were obtained with a Nicolet 360 FT-IR spectrometer, using the KBr pellet method. We collected 64 scans for each spectrum with a 0.2 cm^{-1} resolution.

The britholites surfaces were characterized by scanning electron microscopy (SEM) coupled to X-ray dispersive energies (EDX) by means of a JEOL 6400-LINK AN 10000 microscope.

XRD patterns were collected with a Philips PW 1730 X-ray diffractometer using Cu Kα radiation (step size $2\theta = 0.02$, 10 s of counting time per step) and neutron diffraction patterns were collected on the high-resolution powder diffractometer 3T2 (LLB Saclay, $\lambda = 1.2252$ Å). The 3T2 diffractometer has an array of 20 detectors and an available 2θ domain between 10 and 125.45°, with a step of 0.05°.

Rietveld refinements of the crystal structure were carried out for the three samples. The structural refinements at 300 K were performed simultaneously on the neutron and X-ray diffraction patterns with a 50:50 weighting scheme. The instrumental resolution functions (IRF) of both diffractometers were obtained from well-crystallized standards and taken into account in separated input files. The refinements were performed using the atomic position set and the space group of the HA structure $P6_3/m$, No. 176,[7] by means of the computer program FullProf 2000.[22] In the case of samples B-0.5 and B-1, the preliminary refinements proceeded by allowing a simultaneous presence of Nd at the Ca(1) and Ca(2) sites. However, the refinement of the Nd and Ca occupancies at the Ca(1) position resulted in values very close to 0 and 4 for Nd and Ca, respectively. For this reason we only allowed the presence of Ca atoms at the Ca(1) sites and all the Nd atoms were set at the Ca(2) position. The atomic coordinates of Si and Nd atoms were constrained to be the same as those of P and Ca(2), respectively. Regarding the hydroxyls sites, O(H) and H occupancies were let to vary freely. The occupancy factors are normalized in such a way as to represent the number of atoms in a formula unit.

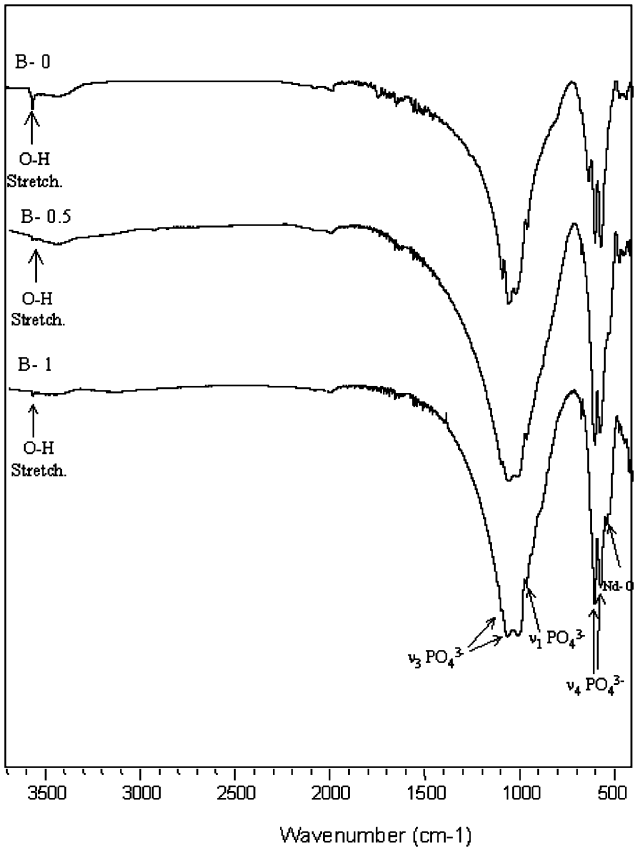

Figure 1. FTIR spectra for samples B-0, B-0.5, and B-1.

By calculating the distortion of the PO_4 tetrahedrons we can get an estimation of the structural distortion. The tetrahedral distortion index was obtained from the calculated data using the relation

$$\mathrm{TDI} = \frac{\sum_{i=1}^{6} |OTO_i - OTO_m|}{6} \quad (1)$$

In this formula, OTO_i denotes the six angles between P and the four O atoms of the phosphate tetrahedron and OTO_m is the average angle (around 109.4°).

Results

Figure 1 collects the FTIR spectra obtained for samples B-0, B-0.5, and B-1. Sample B-0 shows the characteristic

(15) Leventouri, Th.; Bunaciu, C. E.; Perdikatsis, V. *Biomaterials* **2003**, *24*, 4205.
(16) Arcos, D.; Rodríguez-Carvajal, J.; Vallet-Regí, M. *Physica B* **2004**, *350*, e607.
(17) Arcos, D.; Rodríguez-Carvajal, J.; Vallet-Regí, M. *Solid State. Sci.* **2004**, *6*, 987.
(18) Trombe, J. C.; Montel, G. *J. Inorg. Nucl. Chem.* **1978**, *40*, 15.
(19) Serret, A.; Cabañas, M. V.; Vallet-Regí, M. *Chem. Mater.* **2000**, *12*, 3836.
(20) Zhao, H.; Li, X.; Wang, J.; Qu, S.; Weng, J. Zhang, X. *J. Biomed. Mater. Res.* **2000**, *52*, 157.
(21) Okazaki, M.; Tohda, H.; Yanagisawa, T.; Taira, M.; Takahashi, J. *Biomaterials* **1998**, *19*, 611.
(22) Rodríguez-Carvajal, J. *Physica B* **1993**, *192*, 55. For a more recent version see Rodríguez-Carvajal, J. *Recent Developments of the Program FULLPROF*. In *Commission on Powder Diffraction (IUCr) Newsletter 26*, 12−19, 2001, available at http://journals.iucr.org/iucr-top/comm/cpd/Newsletters/. The complete program and documentation can be obtained from the anonymous ftp-site: ftp://ftp.cea.fr/pub/llb/divers/fullprof.2k.

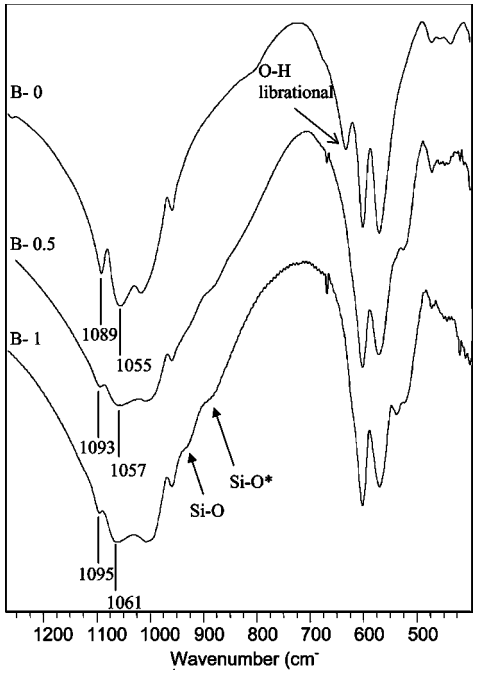

Figure 2. Expanded FTIR spectra between 400 and 1275 cm^{-1}. The frequency values correspond to ν_3 PO_4^{3-} stretching vibration. *The shoulder between 870 and 890 cm^{-1} could overlap the band at 875 cm^{-1} corresponding to HPO_4^{2-} groups.

absorption bands corresponding to a HA phase.[23,24] The intense bands at 1089, 1054, 1007, and 961 cm^{-1} correspond to ν_3 and ν_1 P−O stretching vibration modes. The doublet at 603−567 cm^{-1} corresponds to the O−P−O ν_4 bending mode. The bands at 3570 and 631 cm^{-1} correspond to the stretching and librational modes, respectively, of the hydroxyls groups. Samples B-0.5 and B-1 also show the bands described above. The intensity of the bands assigned to OH groups clearly decreases in these samples. Finally, the absorption bands at 539 cm^{-1} correspond to the Nd−O bond.

Figure 2 is the extended FTIR spectra between 400 and 1250 cm^{-1}. In this figure, two new (shoulder shaped) bands at 931 and 870−890 cm^{-1} occur. These absorption bands are not easy to assign. Some authors have related them to the presence of silicon in the apatite structure.[25] However, the broad shoulder between 870 and 890 cm^{-1} could contain the overlapped band at 875 cm^{-1} corresponding to HPO_4^{2-} groups,[26] as will be explained later.

We can also observe that the ν_3 stretching bands of PO_4^{3-} groups shift to higher frequencies for higher values of *x*. In this way, the band at 1055 cm^{-1} for B-0 shifts to 1057 and 1061 cm^{-1} for B-0.5 and B-1, respectively. Similarly, the band at 1089 cm^{-1} for B-0 shifts to 1093 and 1095 cm^{-1} for B-0.5 and B-1, respectively.

Figure 3 shows the micrographs obtained for the samples surfaces. The mean grain size was calculated using the intercept method.[27] Twenty straight lines were drawn on each

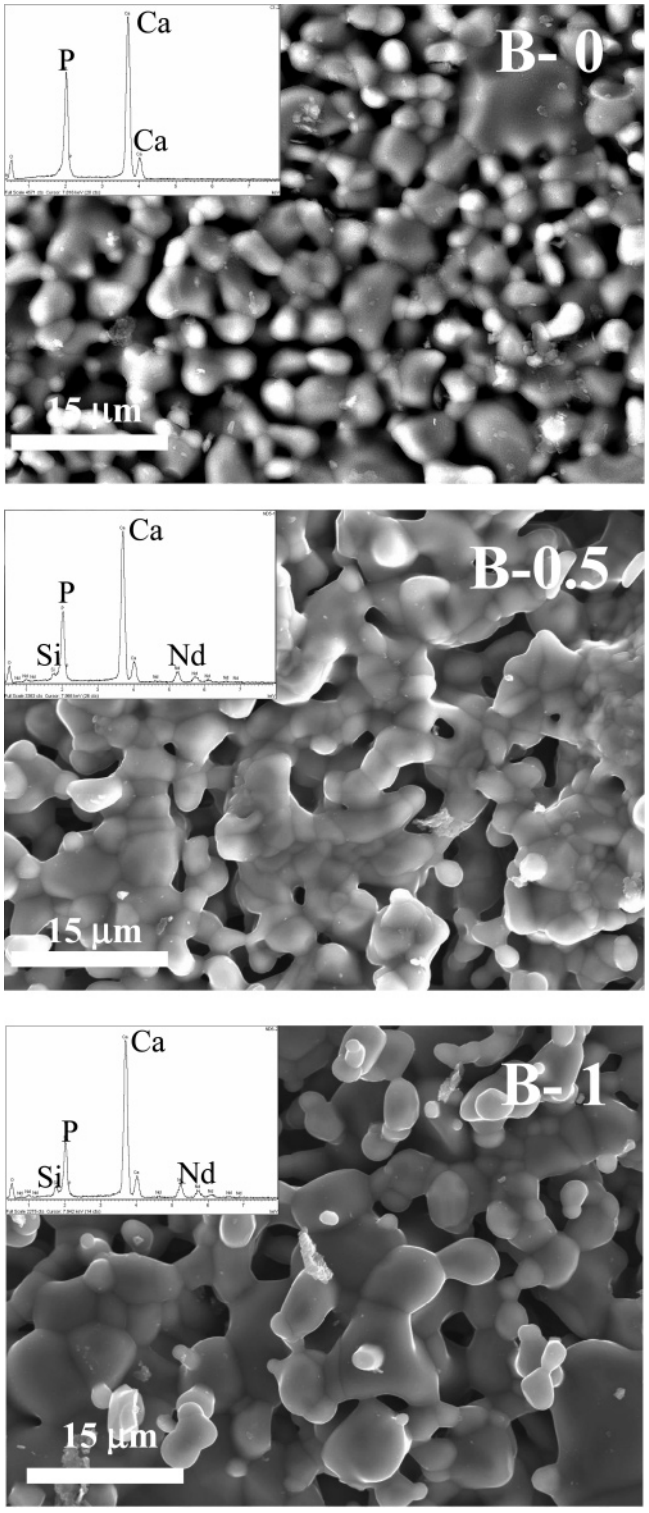

Figure 3. Scanning electron micrographs for the britholites synthesized. The insets show the EDX spectra obtained from the surfaces.

micrograph with different directions. More than 300 grains sizes were considered for each sample. The mean sizes were 2.3 (9), 2.0 (4), and 3.6 (9) μm for B-0, B-0.5, and B-1, respectively. The chemical composition was obtained by EDX spectroscopy during the surface observation. Table 1 collects the results for the three samples, showing experimental values similar to the theoretical ones.

Figure 4 shows the XRD (a) and ND (b) patterns for sample B-0. Both patterns show the diffraction maxima

(23) Fowler, B. O. *Inorg. Chem.* **1974**, *13* (1), 194.
(24) Koutsopoulos, S. *J. Biomed. Mater. Res.* **2002**, *62*, 600.
(25) Gibson, I. R.; Best, S. M.; Bonfield, W. *J. Biomed. Mater. Res.* **1999**, *44*, 422.
(26) Rey, C.; Shimizu, M.; Collins, B.; Glimcher, J. *Calcif. Tissue Int.* **1991**, *49*, 383.
(27) *ASTM E 384-84. Standard Test Method for Microhardness of Materials*; ASTM Committee on Standards: Philadelphia, PA, 1984.

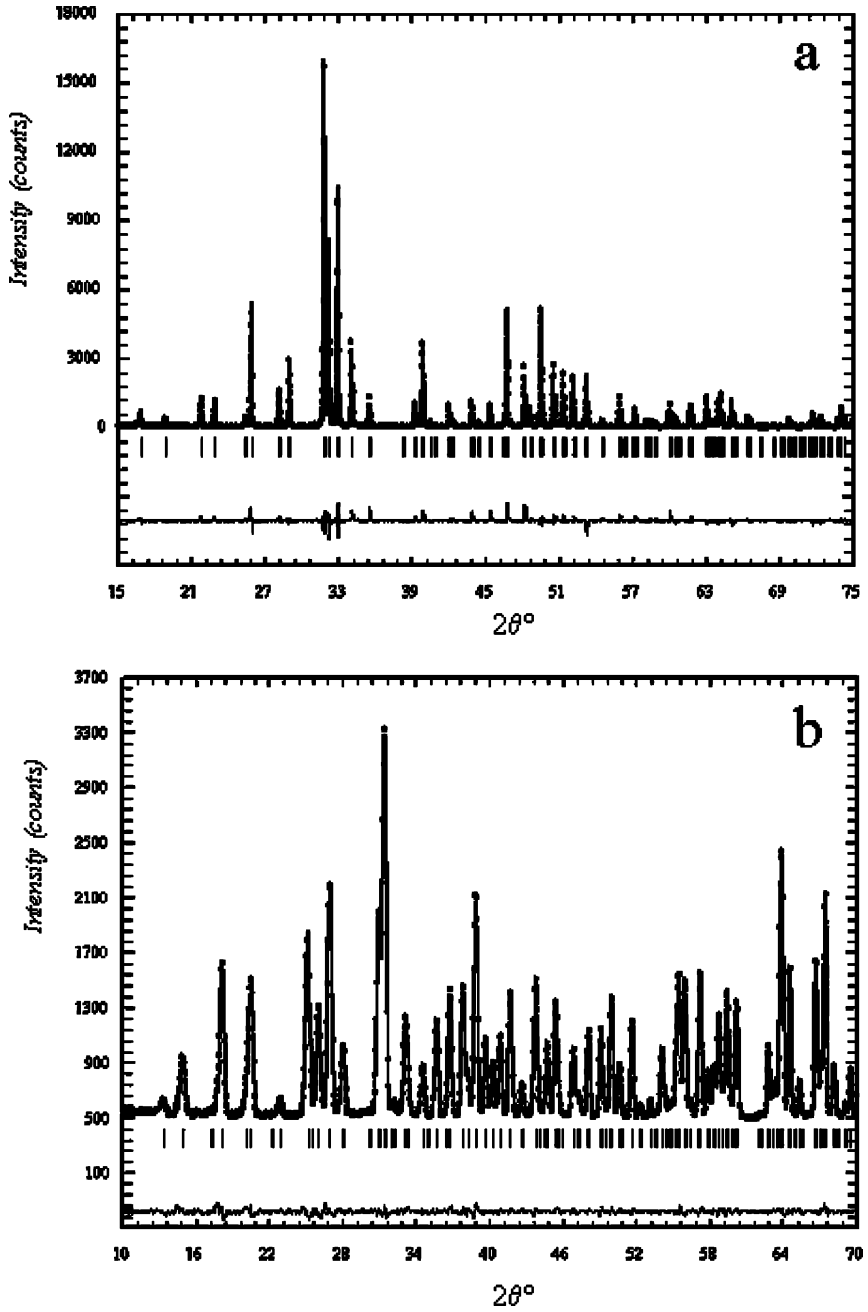

Figure 4. Part of the experimental (dots) and calculated (solid line) powder X-ray (a) and neutron (b) diffraction pattern for sample B-0. The lower trace is the difference between observed and calculated patterns. The vertical lines mark the position of the calculated Bragg peaks for the apatite phase.

Table 1. Atomic Composition (wt %) Obtained by X-ray Fluorescence

sample		Ca	P	Nd	Si
B-0	exp.	38.4(8)	18.6(3)	0	0
	theor.	39.9	18.5	0	0
B-0.5	exp.	37.3(3)	17.4(2)	8.1(4)	0.8(1)
	theor.	36.2	16.2	6.9	1.3
B-1	exp.	35.5(5)	13.0(1)	16.1(5)	2.8(1)
	theor.	32.7	14.0	13.0	2.5

corresponding to a single and well-crystallized apatite phase. Figure 4 also includes the calculated XRD and ND patterns obtained by Rietveld refinement. The difference curve shows the good agreement between the observed and calculated patterns. Table 2 collects the structural parameters and agreement factors calculated by the Rietveld refinement.

Figure 5 shows the XRD (a) and ND (b) patterns for sample B-0.5. Both patterns show the diffraction maxima

Table 2. Atomic Positions, Occupancies, and U_{eq} for Sample B-0[a]

atom	Wyckoff position	*x*	*y*	*z*	occ	U_{eq}
O1	6h	0.3275 (2)	0.4841 (2)	1/4	6	0.0110 (7)
O2	6h	0.5869 (2)	0.4649 (2)	1/4	6	0.0145 (8)
O3	12i	0.3436 (2)	0.2580 (1)	0.0705 (1)	12	0.0224 (6)
O(OH)	4e	0	0	0.1975 (9)	1.92 (3)	0.015 (3)
H(OH)	4e	0	0	0.054 (2)	1.39 (7)	0.023 (8)
Ca1	4f	1/3	2/3	0.0016 (3)	4	0.0103 (9)
Ca2	6h	0.2460 (2)	0.9923 (2)	1/4	6	0.0105 (8)
P	6h	0.3982 (2)	0.3684 (2)	1/4	6	0.0078 (7)

[a] Lattice parameters $a = 9.41844$ (3), $c = 6.88374$ (3). $R_{Bragg\ (apatite)}$ 3.72; Rwp 15.2; Rexp 10.79; χ^2 1.98 (for XRD pattern). $R_{Bragg\ (apatite)}$ 1.55; Rwp 3.96; Rexp 2.59; χ^2 2.33 (for ND pattern).

corresponding to a well-crystallized apatite phase together with two minor phases. These two phases were identified as α-tricalcium phosphate, $Ca_3(PO_4)_2$ (α-TCP), and silicocarnotite, $Ca_5(PO_4)_2SiO_4$. Both phases were introduced in the

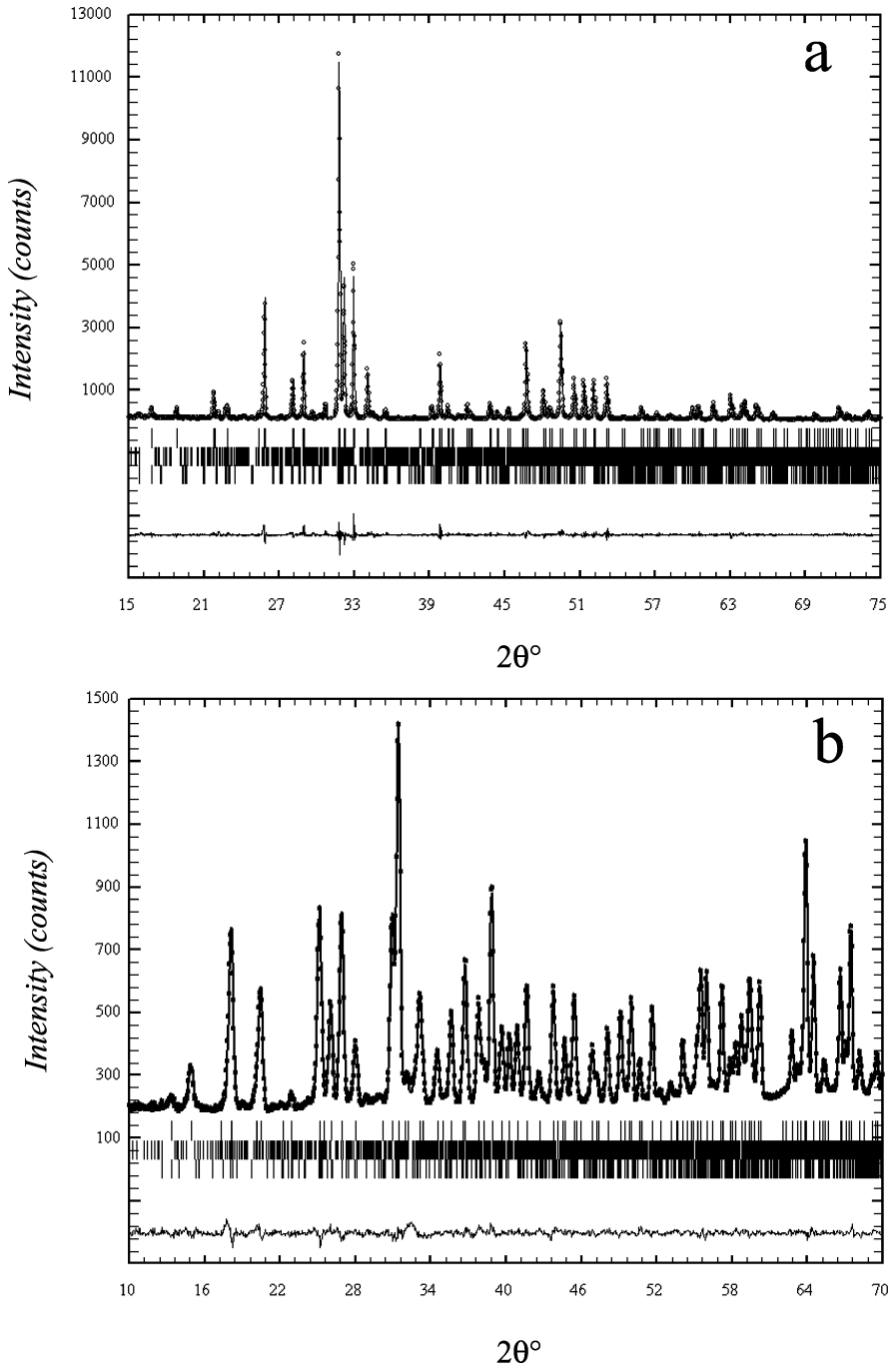

Figure 5. Part of the experimental (dots) and calculated (solid line) powder X-ray (a) and neutron (b) diffraction patterns for sample B-0.5. The vertical lines mark the positions of the calculated Bragg peaks for the britholite, α-TCP, and silicocarnotite phases.

refinement using previously reported structural data.[28,29] Quantitative analysis of the phases was carried out by the Rietveld method,[30] obtaining values of 7.5 and 2.5% for α-TCP and silicocarnotite, respectively. Table 3 collects the structural parameters and agreement factors calculated by the Rietveld refinement for sample B-0.5.

Figure 6 shows the XRD (a) and ND (b) patterns for sample B-1. Together with the main apatite phase, the patterns show two minor phases identified as β-tricalcium phosphate, $Ca_3(PO_4)_2$ (β-TCP),[31] and silicocarnotite. Both

Table 3. Atomic Positions, Occupancies, and U_{eq} for Sample B-0.5[a]

atom	Wyckoff position	*x*	*y*	*z*	occ	U_{eq}
O1	6h	0.3286 (2)	0.4851 (2)	1/4	6	0.0118 (5)
O2	6h	0.5878 (2)	0.4661 (3)	1/4	6	0.0172 (8)
O3	12i	0.3449 (2)	0.2590 (2)	0.0706 (2)	12	0.0242 (7)
O(OH)	4e	0	0	0.2026 (9)	1.65 (2)	0.0170 (7)
H(OH)	4e	0	0	0.050 (4)	0.64 (4)	0.0285 (8)
Ca1	4f	1/3	2/3	0.0001 (3)	4	0.0129 (8)
Ca2	6h	0.2372 (2)	0.9908 (2)	1/4	5.48 (1)	0.0130 (7)
Nd2	6h	0.2372 (2)	0.9908 (2)	1/4	0.52 (1)	0.0130 (7)
P	6h	0.3988 (2)	0.3699 (2)	1/4	5.5 (1)	0.0090 (7)
Si	6h	0.3988 (2)	0.3699 (2)	1/4	0.5 (1)	0.0090 (7)
H2	6h	0.44 (2)	0.06 (2)	1/4	0.12 (4)	0.0172 (8)

[a] Lattice parameters $a = 9.41329$ (5), $c = 6.88808$ (4). $R_{Bragg\ (apatite)}$ 3.72; Rwp 15.2; Rexp 10.79; χ^2 1.98 (for XRD pattern). $R_{Bragg\ (apatite)}$ 1.94; Rwp 5.53; Rexp 3.94; χ^2 1.97 (for ND pattern).

(28) Matthew, M. *Acta Crystallogr*. **1977**, *33*, 1325.
(29) Dickens, B.; Brown, W. E. *Tschermakis Mineral. Petrogr. Mitt*. **1971**, *16*, 1.
(30) Bish, D. L.; Howard, S. A. *J. Appl. Crystallogr*. **1988**, *21*, 86.

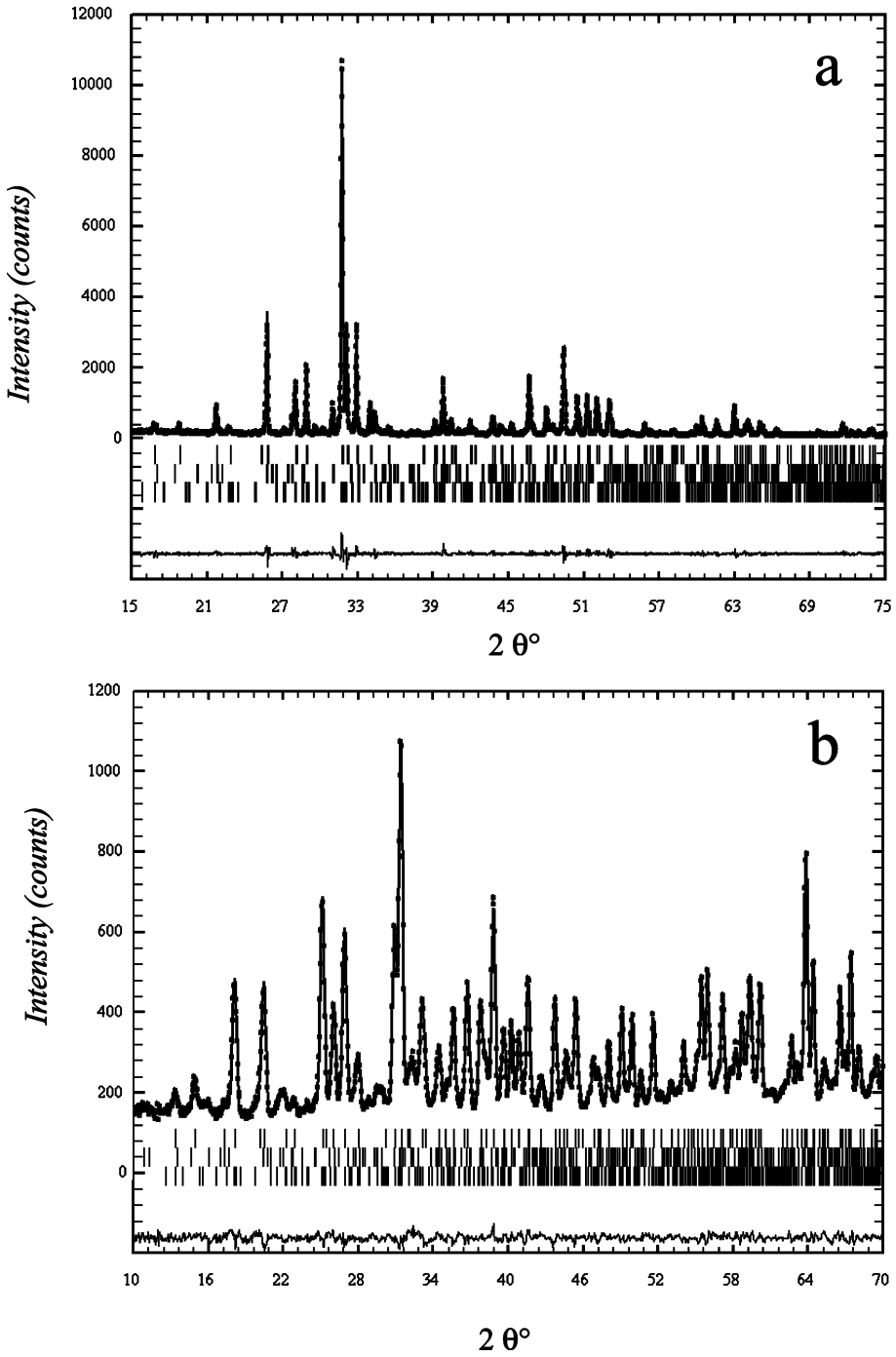

Figure 6. Part of the experimental (symbols) and calculated (solid line) powder X-ray (a) and neutron (b) diffraction patterns for sample B-1. The vertical lines mark the positions of the calculated Bragg peaks for the britholite, β-TCP, and silicocarnotite phases.

phases were introduced in our structural model and quantified. The amounts obtained were 10.8 and 8.4% for β-TCP and silicocarnotite, respectively. Table 4 collects the structural parameters and agreement factors calculated by the Rietveld refinement for sample B-1.

Table 5 collects some significant distances and angles calculated for the britholites studied. We can observe that the higher substitution degree (higher x values), does not result in significant changes in the average P−O distance. The tetrahedral distortion index (TDI) does not show significant change either. However, the Ca(2)−Ca(2) and

Table 4. Atomic Positions, Occupancies, and U_{eq} for Sample B-1[a]

atom	Wyckoff position	x	y	z	occ	U_{eq}
O1	6h	0.3292 (3)	0.4864 (3)	1/4	6	0.0118 (7)
O2	6h	0.5896 (3)	0.4668 (1)	1/4	6	0.0164 (6)
O3	12i	0.3452 (2)	0.2603 (2)	0.0708 (2)	12	0.0206 (5)
O(OH)	4e	0	0	0.207 (1)	1.80 (3)	0.0110 (9)
H(OH)	4e	0	0	0.063 (9)	0.44 (7)	0.0418 (9)
Ca1	4f	1/3	2/3	0.0003 (4)	4	0.0157 (6)
Ca2	6h	0.2319 (2)	0.9907 (3)	1/4	4.93 (2)	0.0138 (3)
Nd2	6h	0.2319 (2)	0.9907 (3)	1/4	1.07 (2)	0.0138 (3)
P	6h	0.4014 (3)	0.3717 (3)	1/4	5.3 (2)	0.0103 (6)
Si	6h	0.4014 (3)	0.3717 (3)	1/4	0.7 (2)	0.0103 (6)

[a] Lattice parameters $a = 9.41862$ (8), $c = 6.89712$ (7). $R_{Bragg\ (apatite)}$ 3.29; Rwp 15.7; Rexp 10.54; χ^2 2.21 (for XRD pattern). $R_{Bragg\ (apatite)}$ 2.68; Rwp 6.98; Rexp 4.94; χ^2 2.00 (for ND pattern).

(31) Yashima, M.; Sakai, A.; Kamiyama, T.; Hoshikawa, A. *J. Solid State Chem.* **2003**, *175*, 272.

Table 5. Significant Distances, Angles, and Tetrahedral Distortion Index for Samples B-0.5 and B-1

	B-0	B-0.5	B-1
P−O1	1.535 (2)	1.526 (3)	1.538 (4)
P−O2	1.539 (3)	1.541 (3)	1.535 (4)
P−O3	1.529 (1)	1.531 (2)	1.534 (2)
P−O average	1.534 (2)	1.532 (3)	1.536 (4)
Ca2−Ca2	4.078 (3)	3.944 (3)	3.861 (3)
Ca2−O(OH)	2.382 (2)	2.300 (2)	2.248 (3)
O1−P−O2	111.3 (2)	111.4 (2)	112.1 (3)
O1−P−O3	111.4 (2)	111.8 (2)	111.0 (2)
O2−P−O3	107.3 (2)	107.0 (2)	107.6 (3)
O3−P−O3	107.8 (1)	107.6 (1)	107.4 (2)
TDI	0.02	0.02	0.02

Ca(2)−O(H) distances clearly decrease as a function of the *x* value.

Discussion

The FTIR study shows the important crystal-chemical changes undergone by the HA structure when Si and Nd replace P and Ca, respectively. Obviously, the absorption bands corresponding to Si−O and Nd−O bonds appear more intense when the *x* value increases. The lower intensity of the O−H stretching band and the removing of the O−H librational mode for B-0.5 and B-1 point out a strong decrease of the hydroxyl content for these two samples. The FTIR spectra also show a shift toward higher frequencies for the ν_3 stretching vibration band of PO_4^{3-} groups. Baddiel and Berry[32] suggested weak hydrogen bonding of the OH··· O−PO_3 type may occur in HA. The lower H content in B-0.5 and B-1 would lead to a lower degree of PO_4 perturbation, which can be reflected in the PO_4 vibrational frequencies. The hydrogen bonding debilitates the O−PO_3 bond, so the lower the H content the higher the O−P frequency vibration, as can be seen for B-0.5 and B-1.

Sample B-0.5 contains α-TCP, $Ca_3(PO_4)_2$, and silicocarnotite, $Ca_5(PO_4)_2SiO_4$, as secondary phases. Since these two phases do not contain Nd, this element must be slightly in excess in the obtained britholites. Actually, the Nd occupancy, 0.52, is slightly higher than the theoretical one, 0.50, although this difference can be considered negligible.

Sample B-1 shows a higher amount of secondary phases, leading to a higher alteration of the britholite composition with respect to the theoretical one. In this case, the britholite contains more Nd (1.07 vs 1.00) and less Si (0.7 vs 1) compared with the theoretical values.

Since the chemical composition at the *4e* Wyckoff position is one the most important factors for the apatite reactivity, it is mandatory to understand the changes undergone by the britholites in this site. For sample B-0, the occupancies in *4e* are 1.92 and 1.39 for O and H atoms, respectively. Considering that all the H atoms are taking part of the hydroxyls groups, the *4e* local chemical composition would result in the following:

$$(OH)_{1.39}O_{0.53}\square_{0.08}$$

where □ means vacancies at *4e* position.

Therefore, the obtained apatite is an oxy-hydroxylapatite, which is very likely to appear under our synthesis method. In the same way, we can calculate the local *4e* chemical composition for samples B-0.5 and B-1. From data collected for sample B-0.5 (Table 3), the occupancies are 1.65 and 0.64 for O and H, respectively. The composition at *4e* would be

$$(OH)_{0.64}O_{1.01}\square_{0.35}$$

For B-1, the data collected in Table 4 show occupancies of 1.80 and 0.44 for O and H, respectively, and the *4e* position for this sample would be

$$(OH)_{0.44}O_{1.36}\square_{0.20}$$

These results are in agreement with the data obtained by FTIR spectroscopy and demonstrate that the higher the substitution degree, the higher the stability of the oxyapatite phase. Serret et al.[19] have reported on the oxyapatite stabilization by nonisoelectrical substitution of La^{3+} for Ca^{2+} cations. These authors reported on the vacancies formation at the *4e* Wyckoff position due to this substitution. The substitutions proposed in our britholites are almost isoelectronic (they are slightly Nd enriched), but the oxyapatite stabilization also occurs.

The Si substitution for P does not lead to significant changes in the PO_4 tetrahedra structure (Table 5). The average distances and the tetrahedral distortion remains the same when the *x* value increases. However, the Nd^{3+} incorporation into the Ca(2) position leads to a decrease of the triangles sides formed by the Ca(2) around the *c* axis (Figure 7). The cations at Ca(2) positions get closer to the OH^- groups, as it is reflected in the decrease of the Ca(2)−O(H) distance as a function of the Nd^{3+} content. This approaching of the cations at Ca(2) toward the OH positions agrees with the O^{2-} for OH^- substitution. The Nd^{3+} substitution for Ca^{2+} leads to an increase of the positive electrical charge around the OH^- or O^{2-} position and the oxyapatite is stabilized. It is well-known that HA synthesized at high temperatures loses the hydroxyls at temperatures over 800 °C,[18] leading to oxyapatite formation. This compound is

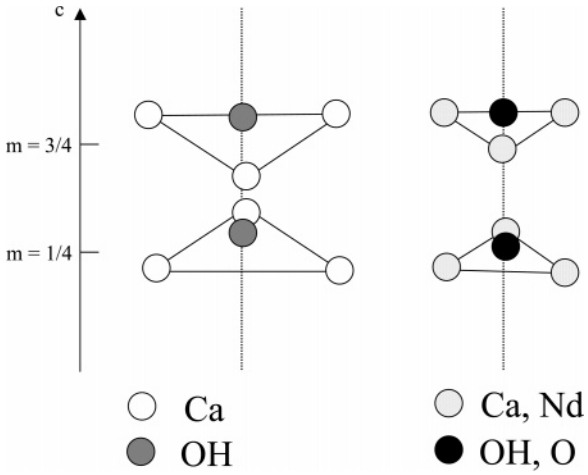

Figure 7. Scheme of the region around the *c* axis for hydroxylapatite (left) and neodymium britholite (right). The two Ca(2) triangles rotated 60° and the *4e* anion are shown. For neodymium britholites the Ca^{2+} and Nd^{3+} at Ca(2) are closer to the OH^- and O^{2-} anions at *4e* when compared with HA.

(32) Baddiel, C. B.; Berry, E. E. *Spectrochim. Acta* **1966**, *22*, 1407.

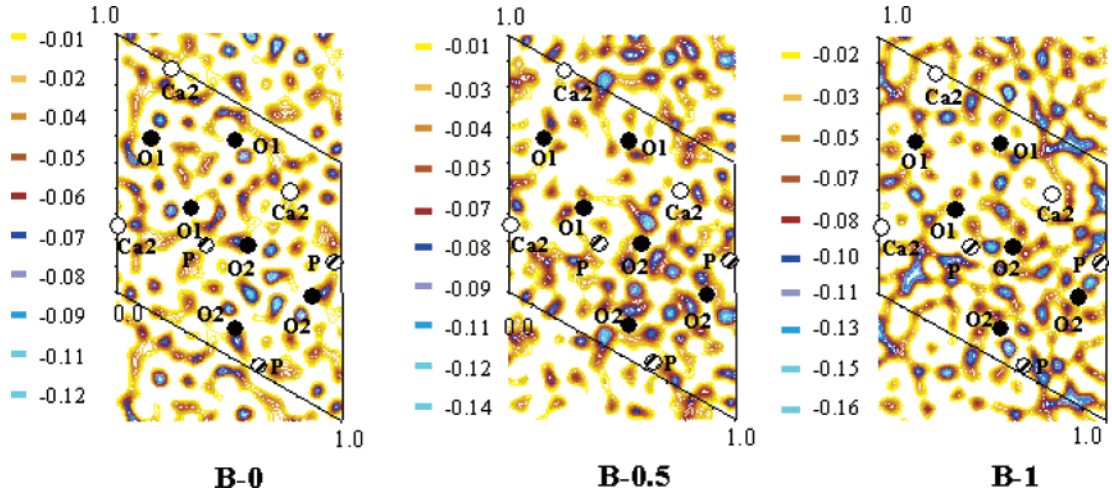

Figure 8. Difference Fourier maps for neutron SD in B-0, B-0.5, and B-1. The negative SD (in blue) corresponds to H atoms (see text). Projection over the mirror plane sited at 0 0 $^1/_4$.

unstable and during cooling under air atmosphere is partially hydroxylated resulting in an oxyhydroxyapatite phase. Our results clearly show that higher values of *x* stabilize the oxyapatite phase. At this point, we must take into account the bigger grain size in sample B-1, because it could also contribute to a lower hydroxylation recovery during cooling.

The local chemical composition at the *4e* Wyckoff position, calculated from the occupancies, would lead to an excess of negative charge in the britholites. If our britholites were fully hydroxylated, the two OH^- groups would provide a local charge of −2. However, due to the presence of O^{2-}, the charges at the *4e* positions would be −2.45, −2.66, and −3.16 for B-0, B-0.5, and B-1, respectively. Vacancies are created in this crystallographic site but this mechanism is not enough. A second mechanism must occur to keep the electrical balance. Figure 8 represents the scattering density Fourier difference maps obtained from the structural models proposed for each sample. The projection over the mirror planes, normal to [0 0 1] direction and sited at $^1/_4$ and $^3/_4$ of the *c* axis, clearly show negative scattering density positions close to the O2 atoms. These sites correspond to H atoms, the only ones that have negative Fermi lengths in these compounds. Since neutron diffraction indicates the presence of H atoms associated with PO_4^{3-} groups, the formation of HPO_4^{2-} groups can be proposed as a hypothesis. In the same way that O^{2-} is partially hydroxylated, following

$$O^{2-} + H_2O \leftrightarrow 2\ OH^-$$

PO_4^{3-} groups could also react as

$$PO_4^{3-} + H_2O \leftrightarrow HPO_4^{2-} + OH^-$$

This mechanism would be in agreement with the negative density, which increases with the *x* values and points out a higher presence of HPO_4^{2-} with the substitution degree. In this way, the substitution of HPO_4^{2-} for PO_4^{3-} would compensate the charge difference. The presence of small amounts of HPO_4^{2-} could be confirmed by FTIR as a low intense band at 875 cm^{-1}. However, the low intensity of this band and the overlapping with the Si−O band do not allow it to be observed clearly in the FTIR spectra.

Conclusions

Britholites of chemical composition $Ca_{10-x}Nd_x(PO_4)_{6-x}(SiO_4)_x(OH)_2$ have been obtained by the ceramic method. These materials can be used as models for the study of ceramic matrixes for nuclear waste storage.

The SiO_4^{4-} for PO_4^{3-} substitution has negligible effect on the PO_4 tetrahedrons.

The Nd^{3+} for Ca^{2+} substitution leads to the stabilization of the oxyapatite phase as well as important structural changes around the OH sites.

The presence of H atoms associated with PO_4^{3-} groups indicates the formation of HPO_4^{2-}, which could contribute to the charge balance.

CM0488231